Jordan Journal of Civil Engineering, Volume **19**, No. **3**, **2025**
DOI: https://doi.org/10.14525/JJCE.v19i3.04

Jordan Journal of Civil Engineering

Journal homepage: https://jjce.just.edu.jo

Strength Meso-correlation in Cement-modified Luoyang Expansive Soil under Dry-Wet Cycles

Yugang Zhang [1]***, Jianjun Ma*** [1,2]****, Chaosheng Wang*** [1,2]***, Shukai Cheng*** [1]

[1] *School of Civil Engineering and Architecture, Henan University of Science and Technology, Luoyang 471023, Henan Province, People's Republic of China.*
[2] *Henan Province Engineering Technology Research Center of Building Safety and Protection, Luoyang 471023, Henan Province, People's Republic of China. * Corresponding Author. E-Mail: majianjun@haust.edu.cn*

ARTICLE INFO

Article History:
Received: 13/1/2025
Accepted: 20/4/2025

ABSTRACT

Shear strength and crack characteristics are crucial factors in determining the engineering properties of expansive soils. In this study, direct shear tests, triaxial shear tests, and crack development tests were implemented to assess the impacts of cement content and dry-wet cycles on the mechanical behavior of expansive soil. The full-surface fracture indices of the triaxial specimens were extracted, and a comprehensive fracture index was calculated. Subsequently, a Support Vector Machine (SVM) model was established to analyze the development of cohesion. The findings indicated that the shear strength and its parameters decrease as the frequency of dry-wet cycles increases, and they initially rise and then fall with the increase in cement content. The maximum shear strength occurs at a cement content of 6%-8%. The correlation between comprehensive fracture index and strength index is better than that of single fracture index, and the correlation between average crack width is the strongest. The support vector machine model is established by replacing the average width of cracks with dry-wet cycle frequency. The model has a small prediction accuracy error, strong adaptability, and high potential. The findings of this study indicate that crack index analysis can effectively simulate the cohesion of expansive soils, demonstrating significant practical potential for engineering construction in expansive soil regions. This approach provides important theoretical support and technical guidance for construction practices in areas characterized by expansive soils.

Keywords: Improved Luoyang expansive soil, Shear strength, Dry-wet cycles, Macro-to-mesoscopic correlation analysis, Support vector machine.

INTRODUCTION

Expansive soil is a soil variety in which the clay content largely comprises hydrophilic minerals, such as montmorillonite, illite, and kaolinite. These soils exhibit high sensitivity to variations in environmental moisture and temperature, characterized by significant water absorption and subsequent expansion, as well as pronounced water loss and resultant shrinkage (Zhao et al., 2019; Luo et al., 2024; Guo et al., 2024). Under the repeated effects of wetting and drying cycles, the internal micro-cracks within expansive soil progressively propagate and widen, leading to a degradation of its shear strength and mechanical properties. This degradation can readily result in various geological risks, including structural settlement and slope failures, presenting considerable threats to infrastructure and safety (Attah et al., 2022; Duan et al., 2024; Almuaythir et al., 2024). Over the past several years, the intensification of harsh weather conditions has led to a sharp increase in the damage caused by expansive soil, significantly impacting infrastructure construction. Consequently, research into the associated issues has become an indispensable topic in the context of national development.

To mitigate the hazards of expansive soil, the engineering field commonly employs the technique of using admixtures for improvement (Karkush et al., 2020; Al-An et al., 2021). Melese et al. (2022) studied the improvement of expansive soil using volcanic cinders, and the results indicated that a 20% volcanic cinder content yielded the best improvement effect. Jemal et al. (2025) investigated the effects of fine cinder gravel and waste marble dust on the stability of expansive soil, using Jimma Town as a case study. Zhang et al. (2024) demonstrated through experiments that with a cement content of 7%, the free expansion rate of the improved soil decreased, while the compressive strength and shear strength initially increased and then decreased. Wang (2024) indicated that the addition of cement reduces the particle size distribution of expansive soil and enhances the stability of the soil mass. Chiu et al. (2024) studied the performance of expansive soil improved with a combination of cement and silica fume. Chu et al. (2022) conducted experiments using calcium carbide slag to improve expansive soil and found that it significantly enhances the compressive strength and increases the water stability coefficient of expansive soil. Eldin et al. (2022) investigated the improvement of expansive soil using lime sludge and sodium chloride and discovered that these admixtures notably reduce the free swell index of the soil. Habal et al. (2024) found that the California Bearing Ratio (CBR) value for expansive soil improved by blast furnace slag increased by 37 times. Aneke et al. (2024) and Gunarti et al. (2023) reported that incorporating fly ash significantly enhanced the CBR of expansive soil while reducing its expansibility and compression coefficient. Janani et al. (2022) demonstrated that the strength and stiffness of expansive soil are significantly boosted by incorporating bentonite. Zhou et al. (2022) and Pachideh et al. (2021) conducted comprehensive evaluations on lime-improved expansive soil to assess its strength and stability. They found that the swelling behavior of the treated soil significantly decreased, while its compressive strength markedly increased. Shivanshi et al. (2022) used gypsum and lime to improve expansive soil and observed that the free expansion rate, expansion pressure, and plasticity index of the treated soil decreased, while the Unconfined Compressive Strength (UCS) significantly increased. Vanessa et al. (2023) utilized limestone mining waste to stabilize Brazilian expansive soil, noting that the expansion pressure and expansion rate gradually decreased. Mobarezi et al. (2024) and ALi et al. (2021) employed enzyme-induced calcium carbonate crystallization technology for soil improvement. They found that the calcium carbonate content in the improved soil doubled, the swelling potential significantly decreased, and the unconfined compressive strength was notably enhanced.

With the advancement of expansive soil research, numerous scholars have identified the occurrence of cracks as a primary element contributing to the reduction in expansive soil strength and the deterioration of its mechanical properties (Xu et al., 2024; Liu et al., 2024; Dinan et al., 2022; Zhu et al., 2024). Zhao et al. (2024) investigated the impact resulting from moisture content, compaction degree, and other factors on the crack evolution mechanism of expansive soil. Dai et al. (2024) assessed the development of fractures using soil resistivity measurements and found that average width and crack area ratio diminished rapidly as soil depth increased. Huang et al. (2019) utilized PCAS software to extract characteristics, such as the joint number, crack number, and other crack indicators of expansive soil. Guo et al. (2024) calculated the volumetric crack rate and found that the time-dependent changes in the planar crack rate in different environments matched the logistic growth model. Sun et al. (2023) conducted a quantitative assessment of the crack characteristics of undisturbed expansive soil using X-ray scanning technology. Han et al. (2024) assessed the influence of rainfall and evaporation on cracks in expansive soil and discovered that with increasing cycle times, irreversible pore alterations occurred, ultimately resulting in scattered harm in the soil. Zhou et al. (2024) found that with the dry-wet cycles becoming more frequent, the crack parameters initially heightened and then stabilized, while the shear strength gradually decreased. Zhang et al. (2024) analyzed the fracture development of rubber-modified expansive soil subjected to freeze-thaw cycles. They discovered that incorporating 5% rubber powder significantly reduced the complexity of fracture evolution and the surface fracture rate.

Existing research primarily focused on strength analysis and fracture development, providing crucial references for engineering practice. However, less attention has been given to the extraction and analysis of side cracks, and there is a lack of methods for calculating the full-surface cracks of specimens. Additionally, the internal relationship between the strength variation patterns of expansive soil and its fracture evolution mechanisms remains underexplored, leading to certain limitations in practical applications. Therefore, this study uses cement-modified Luoyang expansive soil as the research object. It compares and analyzes the shear strength and strength index changes of the altered expansive soil under wet-dry cycles. It also extracts the crack information from the top surface and side of the specimen, calculates the comprehensive crack index, and verifies the superiority of the comprehensive crack index through grey relational analysis. A correlation model was established to quantitatively characterize the relationship between fracture evolution and soil strength parameters by substituting the frequency of drying and wetting cycles with the average crack width. The findings of this study will provide a deeper understanding of the variations in shear strength and crack development patterns of altered Luoyang expansive soil under dry-wet cycles. This study will also explore the correlation between crack progression and the resilience of expansive soil, providing a basis for predicting the strength indices of cement-stabilized expansive soil in engineering applications.

TEST SUMMARY

Test Materials and Devices

The soil used for the experiment was sourced from Luoyang expansive soil, obtained from Mengzhuang village, Xin'an county, Luoyang city. The grain size gradation curve of the Luoyang expansive soil illustrated in Figure (1) was obtained through laboratory tests. The main physical properties are outlined in Table 1. The liquid limit and plastic limit of Luoyang expansive soil are both lower than those of expansive soils from other regions, indicating that this type of soil is more vulnerable to variations in water content and is more likely to cause safety incidents. Therefore, its modification has a greater practical value. The free swelling ratio was determined to be 50.32%. According to the classification standards of building codes, it is classified as a weakly expansive soil and named Luoyang expansive soil. The main focus of this study is to promote rural revitalization and contribute to the construction of harmonious villages. The research findings will primarily be applied to rural development in Luoyang city. Given the characteristics of small-scale rural projects, simple construction techniques, and high economic requirements, there is an urgent need to develop low-cost and easy-to-operate expansive soil improvement technologies suitable for rural construction. Due to the convenient sourcing, low cost, and strong adaptability of cement, as well as its simple operation, stable improvement effects, and minimal performance degradation, this study uses cement as the improvement material. The modification material selected was Tongli composite Portland cement P C 42.5.

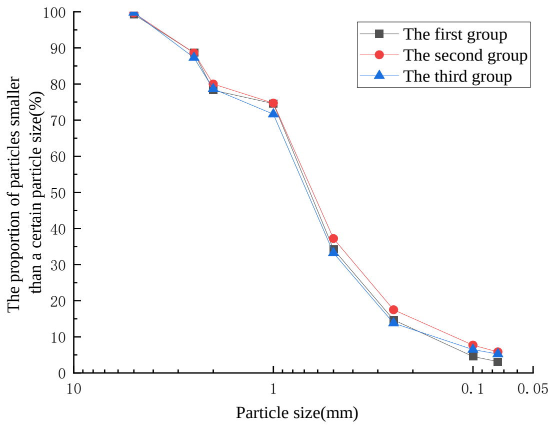

Figure (1): Particle grading curve

Table 1. Expansive soil properties table

Liquid limit (%)	Plastic limit (%)	Plasticity index	Optimum moisture content (%)	Maximum dry density (g/cm^3)	Natural moisture content (%)	Natural dry density (g/cm^3)	Free swelling ratio (%)
37.20	15.42	21.78	15.80	1.730	10.71	1.630	50.32

The direct shear test was conducted using a Z-J type strain gauge direct shear apparatus (produced by Nanjing Ningxi Soil Instrument Co., Ltd.). The shear rate was established at 0.8 mm/min, while the vertical pressures applied during the test were 100 kPa, 200 kPa, 300 kPa, and 400 kPa, respectively. The unconsolidated undrained triaxial shear test was conducted using a strain-controlled triaxial testing apparatus (produced by Zhuode Instrument Equipment Co., Ltd. in Shanghai). The shear rate for this test was also 0.8 mm/min, and the confining pressures were established at levels of 100 kPa, 200 kPa, and 300 kPa. The testing procedures strictly followed the GB/T 50123-2019 "Standard for Geotechnical Testing (2019)." These specific pressures were chosen to assess the response of Luoyang expansive soil under different stress conditions, enabling a thorough examination of the soil's mechanical responses under different pressure scenarios. The samples after the dry-wet cycles were photographed using a Sony Z50 camera, which has a maximum resolution of approximately 20.88 million pixels. The camera was positioned at a height of 50 cm from the samples, with automatic focus.

Test Methods

Sample preparation utilized the compaction and remolding method. The soil specimen is dehydrated and screened through a 2-mm mesh to achieve consistent particle dimensions. Five sets of altered soil specimens were created, encompassing a range of cement concentrations: plain soil (without additives) and modified soils with 4%, 6%, 8%, and 10% cement, respectively. This study was carried out to examine the influence of varying cement contents on the mechanical behavior of the soil under different conditions. The cement was incorporated using the internal mixing method. The starting moisture level of the modified expansive soil was controlled to 15%, the samples were prepared after being sealed and left undisturbed for 12 hours. The samples extracted using the ring cutter had dimensions of 61.8 millimeters for the diameter and 20 millimeters for the height, with a total of 160 samples prepared for two parallel tests. The triaxial test specimens were crafted with dimensions of 50.0 millimeters for diameter and 80.0 millimeters for height, having prepared 120 samples for two concurrent tests. The curing period for all samples was 14 days.

Given that the preliminary test indicated a saturated moisture content of 20% for the plain soil and a natural moisture content of 10.7% for Luoyang expansive soil, the moisture content range for the dry-wet cycles was set between 10% and 20%. The number of dry-wet cycles was established at 0, 1, 3, and 5. Before starting the dry-wet cycles, each sample was weighed, numbered (with a starting moisture content of 15%), and the weights were calculated for each sample at 20% moisture content (after wetting), 10% moisture content (after drying), and at the end of the cycle (15% moisture content). The extent of the dry-wet cycles was assessed based on the sample weights. Figure (2) illustrates the dry-wet cycle process, where the sample is wetted to 20% moisture content, dried to 10% moisture content, and then wetted back to 15% moisture content, constituting one complete dry-wet cycle.

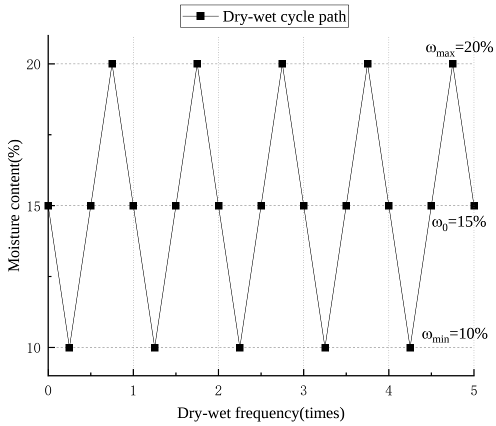

Figure (2): Drying-wetting cycle path

During the dry-wet cycling process, an electronic balance was used to strictly monitor and control the sample mass. To simulate real environmental conditions, the dehumidification process was conducted using a thermostatic electric drying oven set to 40°C for low-temperature drying. The sample weight was measured every 30 minutes during the dehumidification process. For the humidification process, the ring cutter samples were placed on absorbent filter paper and permeable stones alternately, utilizing the capillary absorption of the permeable stones. The triaxial samples were wrapped with filter paper and sponge, and water was evenly sprayed on the sponge using a spray bottle to facilitate water absorption. The sample weight was tested every 15 minutes during the humidification process. After each humidification or dehumidification cycle, the samples were sealed and left to stand for 24 hours to ensure stability in their conditions.

ANALYSIS OF TEST RESULTS

Strength Analysis

Figure (3) presents the association between the variability in shear strength and the count of drying-wetting cycles, as well as the cement content, as observed in the direct shear test. As indicated by Figure (3a), when the cement content is 0%, the shear strength observed in the direct shear test progressively decreases as the count of drying and wetting cycles rises. The attenuation amplitude of the shear strength of 0-1 drying-wetting cycles is large, and then, the attenuation amplitude slows down. As depicted by Figure (3b), when there were no drying-wetting cycles, the shear strength results from the direct shear test initially rose and then fell as the cement content increased, reaching its maximum value at a cement content of 6% to 8%. When the frequency of wetting-drying cycles and constant vertical load are kept constant, the shear strength of the sample is 8%, 6%, 10%, 4% and 0% from high to low according to the cement content. It is evident that the shear strength of the sample significantly rises with the application of vertical stress, showing obvious linear characteristics, and the correlation coefficients after linear fitting are greater than 0.95, indicating that the internal friction angle and cohesion force calculated using the Coulomb formula are highly reliable.

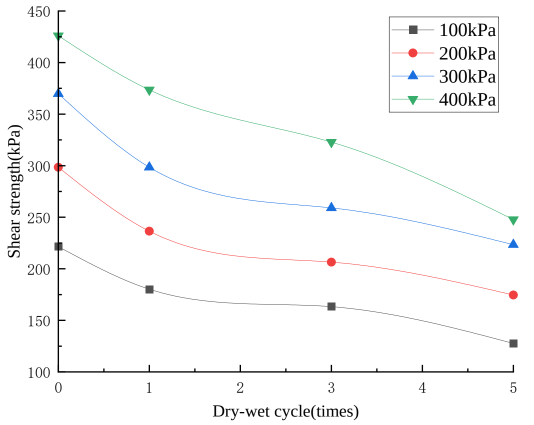

(a) Shear strength - dry and wet cycle change curve at 0% cement content

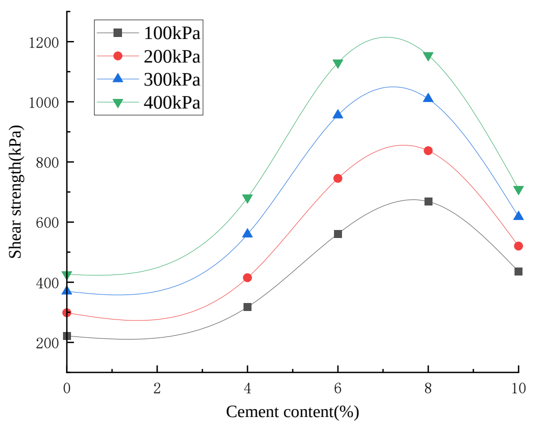

(b) Shear strength - cement content change curve under 0 dry-wet cycles

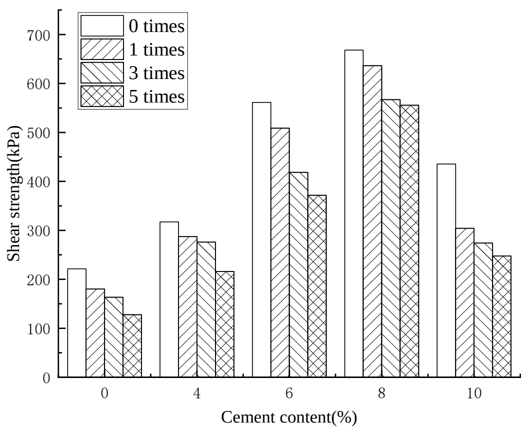

(c) 100kPa direct shear test shear strength

Figure (3): Shear strength change curve of direct shear test

Figure (4) depicts the variation curve of shear strength from triaxial shear tests in relation to the cycle count of drying-wetting cycles and the cement mix ratio. As indicated by Figure (4a), when the cement content is 0%, the triaxial shear strength shows a stepwise diminishing with each dry-wet cycle, but the overall reduction remains small. The maximum attenuation was 94.1kPa and the maximum attenuation rate was 31.2%.

Observing Figure (4b) reveals that the variation pattern of shear strength derived from the triaxial shear test echoes the shear strength changes noted in the direct shear test. As cement content rises, shear strength initially ascends before declining, reaching its peak at a cement content of 8%.

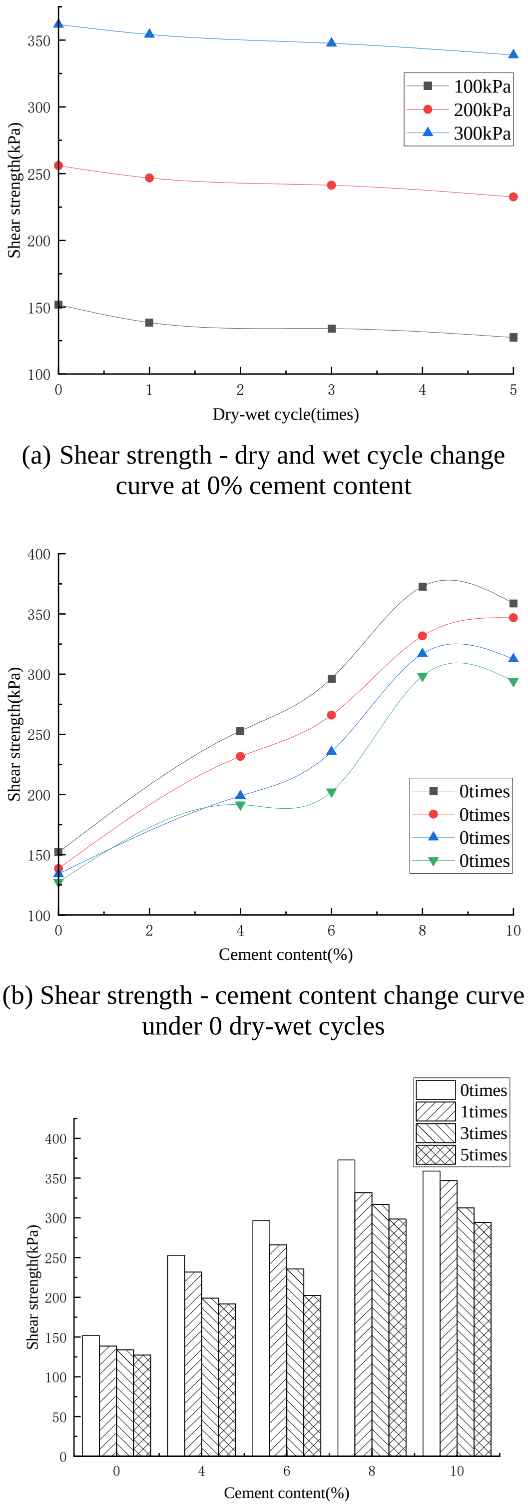

(c) 100kPa direct shear test shear strength

Figure (4): Shear strength variation curve of triaxial shear test

Cement can fill the pores of soil and enhance the consolidation and compactness of soil. The hydration reaction with expansive soil and water can produce hydration products, which can effectively strengthen the inter-particle cohesion and boost the soil's shear resistance. An excessive amount of cement decreases the moisture content within the soil, affects the stability of hydrate, easily forms uneven slurry, and results in alterations to the soil's pore structure, but negatively affects the shear strength. Dry and wet cycling will lead to soil moisture change, changing the arrangement and structure of soil grains, diminishing the interaction between soil grains and decomposing the hydration products within the soil, resulting in the dissolution of clay minerals, and causing reduced shear strength.

The results indicate that the direct shear strength surpasses the triaxial shear strength under comparable conditions. This result is owing to that the stress state of the sample is different, the elevation of the ring knife specimen is minimal, and the stress distribution is more uniform. The failure of the triaxial specimen during the shear test involves shear failure and volume change, displaying varying strength behaviors. The gradual decrease in shear strength observed in the triaxial shear test is influenced by the size of the specimen.

Analysis of Cohesion and Internal Friction Angle

Figure (5) illustrates the variations of cohesion and internal friction angle of the cement-enhanced Luoyang expansive soil depending on the frequency of dry-wet cycles and the proportion of cement. The dotted line graph represents the internal friction angle, while the bar chart represents the cohesion. According to Figure (5a), with a consistent cement content, the cohesion values from the direct shear test typically decrease with the rise in the count of dry-wet cycles. For the initial cycles (0-3), the change is more pronounced compared to later cycles (3-5). The internal friction angle experiences a progressive decline. Given a consistent frequency of dry-wet cycles, both cohesion and internal friction angle initially increase and subsequently decrease as cement content increases. The maximum cohesion is observed at 8% cement content, while the maximum internal friction angle is observed at 6% cement content. The reason for the aforementioned phenomenon is that cement alters the soil structure and pore characteristics. As the cement content increases, the hydration products of the cement fill the voids between soil particles, enhancing the soil structure and increasing both cohesion and internal friction angle. When the cement content reaches 6%-8%, the hydration reaction and cementing effect of the cement achieve optimal results, effectively filling the gaps between soil particles and forming a denser structure. At this point, the strength and stability of the soil reach their peaks, resulting in maximum friction and cohesion. However, when an excessive amount of cement is added, a phenomenon of cement particle aggregation occurs, forming cement clumps that reduce the overall structural stability of the soil, leading to a decrease in cohesion and internal friction angle. Additionally, excessive cement can weaken the interactions between cement particles, affecting the distribution of moisture in the soil and subsequently impacting the hydration process of the cement, which also leads to a reduction in cohesion and internal friction angle.

From Figure (5b), it can be observed that the trend of cohesion variation in the triaxial shear test with dry-wet cycles is consistent with that observed in the direct shear test, showing a decreasing trend. Nevertheless, the internal friction angle's variation with dry-wet cycles exhibits a less pronounced pattern. The internal friction angle varies differently under different cement contents. For instance, with a 4% cement content, the internal friction angle declines following the sequence of 3, 5, 0, and 1 dry-wet cycles. At an 8% cement content, the reduction in the internal friction angle follows the progression from 1, 3, 0, and 5 dry-wet cycles. These variations are attributed to the different internal states of the samples under confining pressure, which result in different internal friction angles and performance characteristics.

The research results also indicate that the impact of the first three wet-dry cycles on shear strength, cohesion, and internal friction angle is significantly greater than that of the 3-5 subsequent cycles. This is because, during the first three wet-dry cycles, the soil structure of the expansive soil undergoes significant changes. When wet, the increase in moisture between soil particles weakens the interaction forces, leading to the phenomenon of soil expansion; conversely, when dry, the reduction in moisture causes the soil to shrink, and the changes in pore structure significantly affect its mechanical properties. As the number of cycles increases, the re-organization of pores and the migration of moisture gradually stabilize, resulting in a new equilibrium state for the micro-structure and mechanical properties of the soil. Consequently, the effects of subsequent cycles on shear strength, cohesion, and internal friction angle gradually diminish.

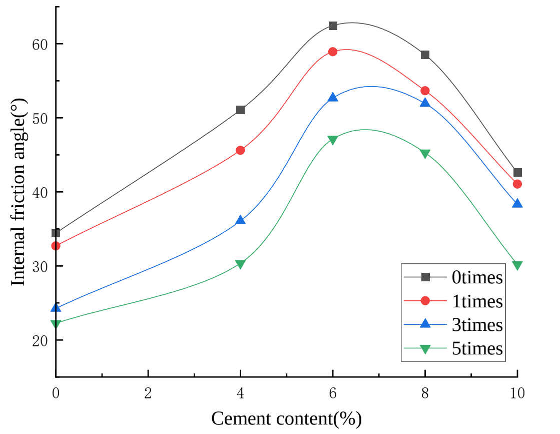

(a) Change curve of internal friction angle in direct shear test

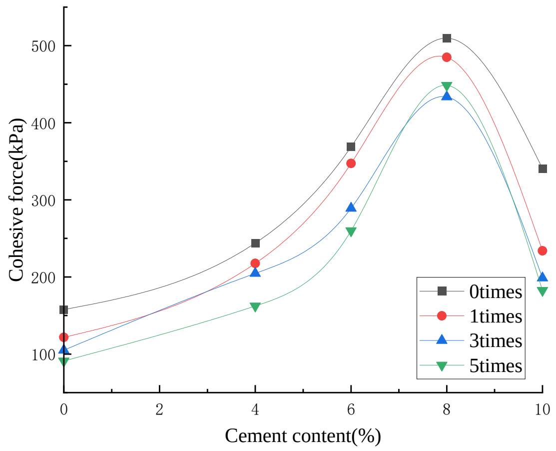

(b) Change curve of cohesion force in direct shear test

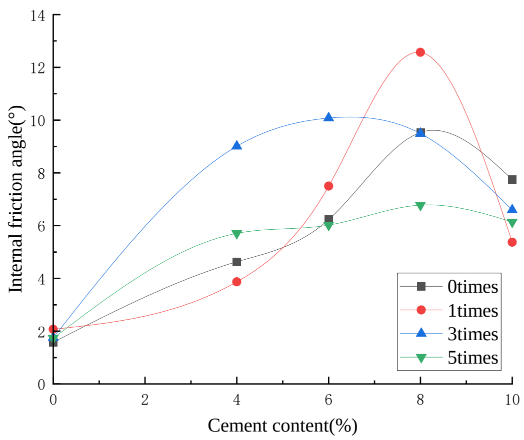

(c) Change curve of internal friction angle in triaxial shear test

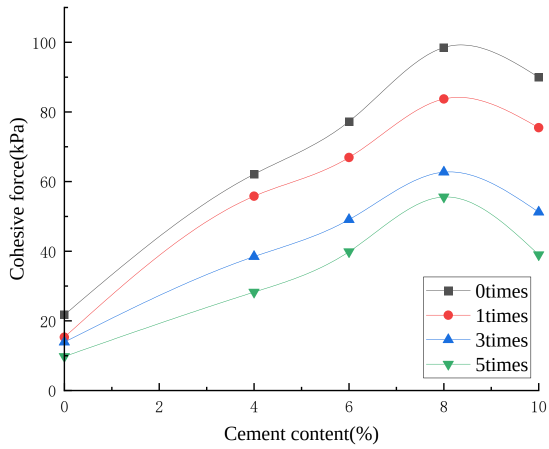

(d) Change curve of cohesion force in triaxial shear test

Figure (5): Variation trend of shear strength index

The wetting and drying cycles markedly diminish the inherent bonding strength within the soil, enlarge the spacing between particles, and result in reduced cohesion and a lower internal friction angle. The addition of cement can improve soil density and bonding force, effectively increasing soil cohesion and internal friction angle. As the cement content increases, the binding force between cement particles and the distance between soil grains increase, causing an enhancement in cohesion. However, when the cement content is too high, an excess of cement may result in the soil's structure becoming brittle, which in turn lowers cohesion. The internal friction angle is mainly affected by the interaction between soil particles, their shape, size, and arrangement. The contact and interaction between soil particles are optimized at an appropriate cement content, leading to the maximum internal friction angle. Owing to the effects of sample stress state, size, and testing method, the values for internal friction angle and cohesion as measured by the direct shear test are typically superior to those ascertained by the triaxial shear test.

Analysis of Crack Index

Sony Z50 camera was used to capture images of the triaxial shear samples after the dry-wet cycle. During photography, two incandescent light sources were positioned at a height of 3.0 meters, and the camera was fixed at a height of 50 cm. After automatic focusing, the samples were recorded. The original image is an RGB image. Using the segmentation function in Image-Pro Plus digital image processing software, the iterative adjustment method was used to precisely calibrate the red, green, and blue histogram thresholds of the image (with a threshold adjustment range of 0 to 255). Following this, the image was changed into a binary image, where cracks are represented as black and the background as white. Using the Filters command, methods such as Median filtering (which sorts neighboring pixels by value and takes the middle value, effectively removing salt-and-pepper noise), Low-pass filtering (which removes high-frequency noise from the image while retaining low-frequency information), and Laplacian filtering (an edge detection filter that can be used to sharpen images and enhance edges and clarity) were applied. A suitable radius range was set to remove noise and connect cracks in the image, resulting in a denoised image. The specific process is shown in Figure (6). The crack index of the sample was identified and extracted using Matlab (2022b) software, including Crack area ratio, Total crack length, Average crack width and Fractal dimension.

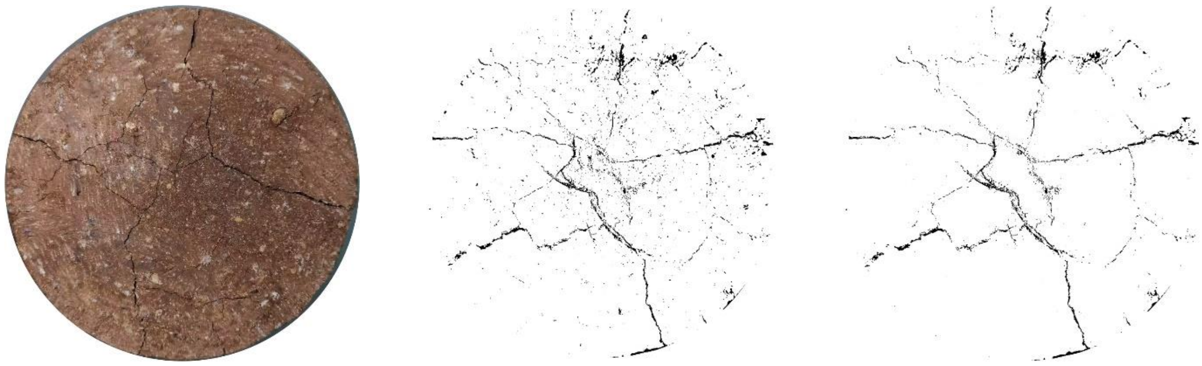

(a) source image (c) binary image (e) denoised image

Figure (6): Image processing process

Both the side fissures and the upper surface cracks of the sample significantly affect its strength characteristics. Therefore, this study first extracts the upper surface crack index and the side crack index of the sample. Since a single crack index cannot uniformly describe the development of fissures, a comprehensive crack index is introduced. The comprehensive crack index is obtained according to the definition of crack parameters, and the specific calculation method is as follows:

$$CAR = (CAR(\mathrm{a}) + CAR(\mathrm{b}))/(TA(\mathrm{a}) + TA(\mathrm{b}))$$
$$TCL = (TCL(\mathrm{a}) + TCL(\mathrm{b}))$$
$$ACW = (ACW(\mathrm{a}) + ACW(\mathrm{b}))/2$$
$$FD = (FD(\mathrm{a}) + FD(\mathrm{b}))/2$$

CAR: Crack area rate; TA: Total area; TCL: Total crack length; ACW: Average crack width; FD: Fractal dimension; a: Upper surface crack index; b: Side crack index.

The progression of fracturing in the sample is depicted in Figure (7). Following the initial dry-wet cycling, the reduction in moisture content induced contraction in the samples, leading to the formation of numerous micro-cracks on the upper surface and fewer, but longer, cracks on the side surface. With the progressive increment of dry-wet cycles, the micro-cracks on the upper surface propagated inward, and primary cracks started to develop on the sample surface, while the side cracks extended outward. As the dry-wet cycles persisted, the primary cracks on the sample surface inter-connected, creating an intricate web of fractures. The crack development in samples with added cement exhibited a similar pattern to that in samples without cement, but the area of cracks and the number of fissures were significantly reduced.

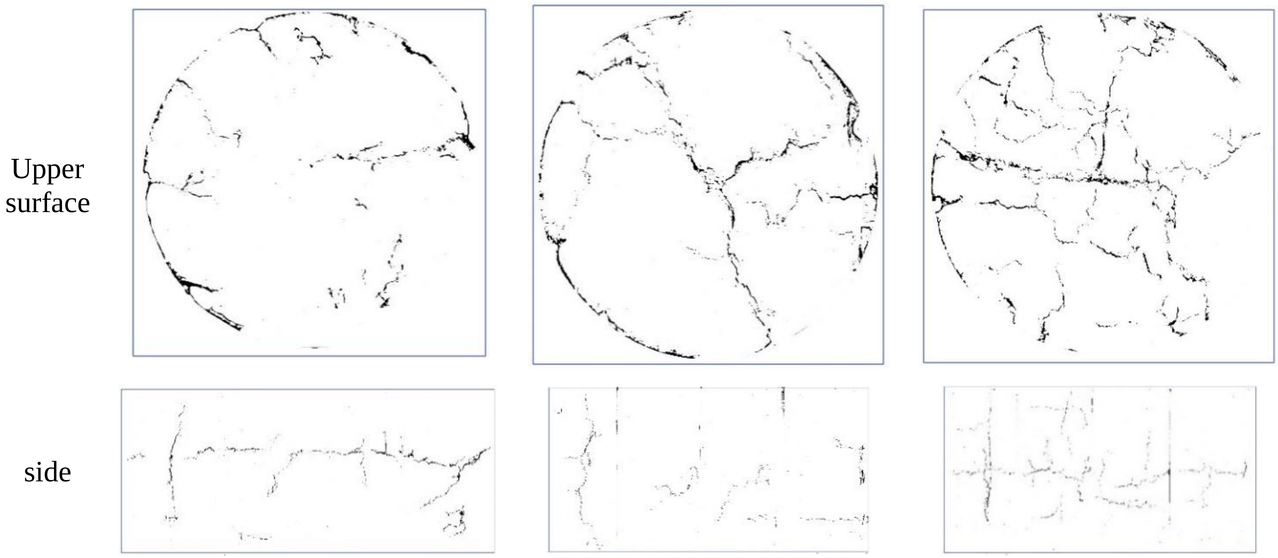

(a) 1 dry-wet cycle (b) 3 dry-wet cycles (c) 5 dry-wet cycles

Figure (7): Crack evolution process of sample

The grey correlation degree approach was employed to assess the correlation between the upper surface crack index, side crack index, and comprehensive crack index in relation to the internal friction angle and cohesion as determined by the triaxial shear test. The computed results are listed in Table 2 and clearly indicate that the comprehensive crack index has a stronger correlation with both the internal friction angle and cohesion compared to a single crack index, verifying the feasibility of the comprehensive crack index. Additionally, the analysis indicated that the average crack width exhibits the strongest correlation with the strength parameter, suggesting that the average crack width has the most significant association with the triaxial shear strength index of improved Luoyang expansive soil. In addition, the average width of the cracks shows a certain correlation with the crack area and the total crack length. Therefore, it is scientifically and reasonably justified for utilizing the average crack width as a criterion for evaluating cracks to assess the triaxial shear strength index.

Table 2. Correlation calculation results

Index	Internal friction angle			Cohesive force		
	Upper surface crack index	Side crack index	Comprehensive crack index	Upper surface crack index	Side crack index	Comprehensive crack index
Crack area rate	0.63	0.62	0.65	0.59	0.72	0.71
Total crack length	0.75	0.66	0.74	0.70	0.72	0.78
Average crack width	0.78	0.74	0.82	0.73	0.73	0.81
Fractal dimension	0.70	0.65	0.71	0.68	0.74	0.78

Figure (8) shows the change trend of comprehensive fracture indices of triaxial shear samples. The sample surface that was not subjected to dry-wet cycling showed no visible cracks. Therefore, the crack index for this sample was recorded as 0, indicating a complete absence of surface damage. The information in Figure (8) reveals that following the initial drying-wetting cycle, there is a significant increase in crack indices, followed by a gradual slowing of changes in these indices. The frequency of cracks demonstrates a distinct upward trend as wet-dry cycles become more frequent and initially diminishes before it rises in response to the augmentation of cement content. The average width of cracks first grows and then diminishes, influenced by more frequent dry-wet cycles and higher cement content. The total crack length undergoes a marked rise in correlation to the rising count of dry-wet cycles, and it starts by diminishing before escalating as the cement content is augmented. The fractal dimension gradually ascends with the frequency of dry-wet cycles mounts, and it incrementally declines in tandem with the rising levels of cement content.

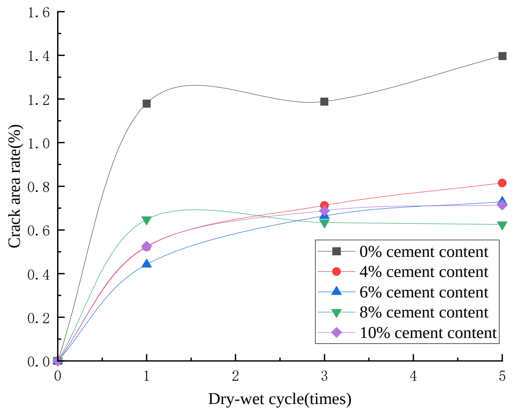

(a) Crack area rate trend chart

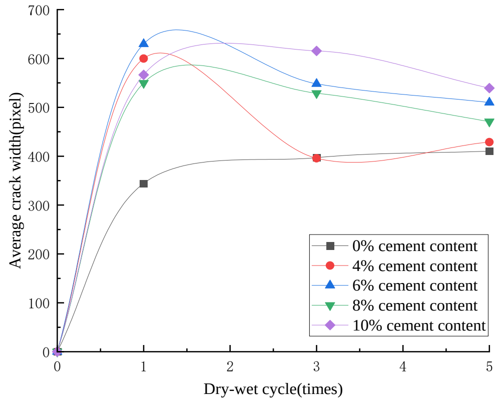

(b) Average crack width trend chart

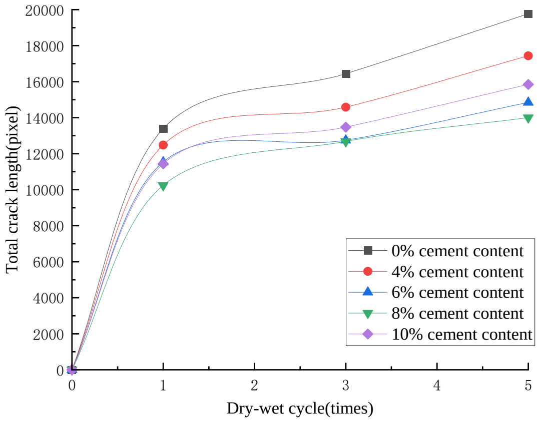

(c) Total crack length trend chart

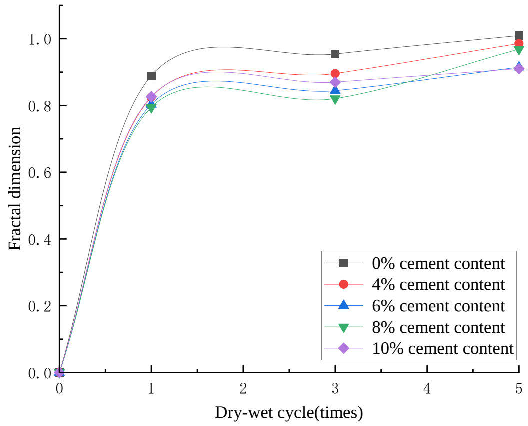

(d) Fractal dimension trend chart

Figure (8): Crack index trend chart

Cracks are caused by tensile stress resulting from soil shrinkage due to water loss. During the initial wetting and drying cycle, the sample remains relatively intact, and subject to tensile forces, numerous micro-cracks are produced with a small crack area. The crack rate, fractal dimension, and total length of cracks are relatively small; however, since the average crack width is the ratio of crack area to total crack length, the average crack width is actually larger. As the soil sample undergoes repeated wetting and drying cycles, the cracks open and close repeatedly, resulting in the compromise of the sample's structural integrity. The number of cracks increases, and the complexity of the cracks deepens, resulting in an increase in crack rate, fractal dimension, and total length of cracks, while the average crack width relatively decreases. Introducing cement can modify the makeup and arrangement of soil particles, resulting in a reduction in crack rate and fractal dimension, as well as a significant decrease in total crack length after experiencing the same extent of wet-dry cycles, while the average crack width relatively increases. Different cement contents have varying effects on soil improvement, leading to different patterns in the changes of crack parameters.

Correlation Model between Crack Index and Cohesive Force

Taking into account the profound effect of dry-wet cycles on crack properties and the difficulty in accurately defining or measuring dry-wet cycles in practical engineering, crack parameters can be used as a substitute for the number of dry-wet cycles. This approach not only aids in assessing changes in the strength parameters of expansive soils in actual engineering scenarios, but also promotes the application of crack research in related engineering fields. Given that the mean crack width exhibits the highest correlation with strength parameters, and the variation pattern of cohesion is more distinct, it can be concluded that the average width of cracks can serve as a substitute for the frequency of dry-wet cycles, thereby studying the correlation between the average width of cracks and the cohesion of expansive soil. A support vector machine (SVM) regression model is employed to predict the relationship between the two. This model can automatically select the optimal parameters, making it suitable for multi-parameter analysis. The core of this method is to find the best hyperplane such that the samples are as close to the hyperplane as possible. The calculation process is as follows:

(1) Data extraction and division: Data is extracted and divided, with cement content, internal friction angle, and average crack width as the input features, and cohesion as the output feature. The dataset is divided into a training set and a validation set.

(2) Grid search is performed to set the best hyper-parameters for the model, including the kernel function (KernelFunction), penalty parameter (BoxConstraint), tolerance parameter (Epsilon), shrinkage period (ShrinkagePeriod), and optimization algorithm (Solver).

(3) A model is created that automatically selects the optimal hyper-parameters, and the optimal parameters are computed.

(4) The optimal parameters are used to train the model and the model is validated using the validation set. Performance metrics are calculated: Mean Squared Error (MSE), Mean Absolute Error (MAE), Root Mean Squared Error (RMSE), and the coefficient of determination (R^2).

Figure (9a) is a comparison diagram of model verification curves. Through the comparison and analysis of the actual values of the validation set with the predicted values of the model, it is evident that there is a high degree of fit between the two, with errors close to zero, indicating that the model verification effect is excellent. Figure (9b) is the performance diagram of the validation set. From the figure, it can be observed that the discrepancy between the predicted and actual values is minimal, with an error range of -12.0 to 16.4. Specifically, 72.2% of the samples have an error distribution within -5 to 5, and 88.9% of the samples have an error distribution within -10 to 10, further verifying the stability and reliability of the model. The mean squared error (MSE) is 40.3, the root mean squared error (RMSE) is 6.3, the mean absolute error (MAE) is 4.4, the coefficient of determination (R^2) is 0.96, the mean error range is 0.28, the standard deviation of the error range is 6.4, the maximum error of the validation set is 16.4, and the minimum error of the validation set is -11.9. The overall error range and statistical indicators demonstrate that the model has a strong ability to explain data variability, excellent model training and validation performance, robust predictive capability and adaptability, and reliable and effective prediction results. This model can provide robust theoretical support and practical technical means for predicting soil strength indices using fracture indices in engineering practice.

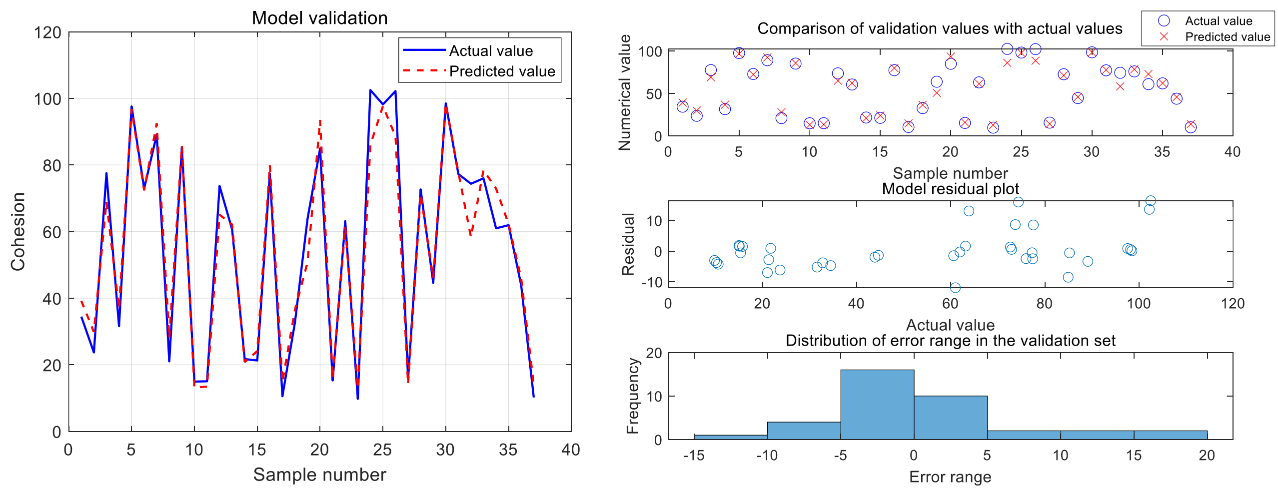

(a) Model validation curve (b) Model error

Figure (9): Model calculation results

CONCLUSIONS

This paper studies the mechanical properties of cement-improved Luoyang weak expansive soil through laboratory tests and constructs a macro-micro support vector machine model. The following main conclusions were drawn.

1. Cement content and dry-wet cycles markedly influence the shear strength of expansive soils. The shear strength of modified expansive soils undergoes a gradual decline with the escalation of dry-wet cycle frequency. With increasing cement content, the shear strength initially rises and subsequently falls, reaching a maximum at a cement content of 6% to 8%. Under identical testing conditions, the shear strength obtained from direct shear tests is notably higher than that obtained from triaxial shear tests. The cohesion and internal friction angle of the improved soil diminish as the frequency of dry-wet cycles rises. With the increase in cement content, the internal friction angle of the improved soil begins by decreasing and increases later.
2. After the first dehydration, micro-cracks emerge on the surface of the sample. As the wetting and drying cycles proceed, crack quantity increases, where the crack width expands and eventually interconnect to form a network of cracks. The progression of cracks is intricately associated with the degree of dry-wet cycling and the effectiveness of cement improvement. Subject to dry-wet cycling, the average cracks width initially increases and then decreases, while the crack density, fractal dimension, and total crack length exhibit a rising pattern. As the proportion of cement within the mixture rises, the crack density and total crack length initially decrease and then increase, the average crack width first rises before declining, and the fractal dimension decreases gradually.
3. The correlation between the comprehensive crack index and the internal friction angle and cohesion is higher than that of a single crack index. Notably, the correlation between the average crack width and cohesion is the strongest. A correlation model established by substituting the average crack width for the frequency of dry-wet cycles features minimal error and robust applicability, rendering it appropriate for use in particular engineering contexts.

Due to limitations in experimental conditions and methods, the effects of wet-dry cycles, cement, and other factors on Luoyang expansive soil still require more in-depth and detailed research. Subsequent studies could include SEM tests to further elucidate the development of micro-cracks, as well as field foundation model tests to verify the actual improvement effects.

Author Contributions

All authors participated in the experimental design and review, as well as the feasibility analysis of the study. Material preparation, experimental operations, data collection and analysis were performed by Yugang Zhang, Jianjun Ma, and Chaosheng Wang. The first draft of the manuscript was written by Yugang Zhang and Shukai Cheng. All authors provided review comments on the manuscript and all authors read and approved the final manuscript.

Data Availability

Enquiries about data availability should be directed to the authors.

Conflict of interests

The authors have no conflict of interests to declare.

Funding

The authors gratefully acknowledge the support of National Natural Science Foundation of China (Grant No. 11502072) and Henan Province Joint Fund for Science and Technology Research and Development (Application-oriented Key Projects) (Grant Nos. 232103810082 and 222102320462).

REFERENCES

Al-Ani, S.M., Karkush, M.O., Zhussupbekov, A., and Al-Hity, A.A. (2021). “Influence of magnetized water on the geo-technical properties of expansive soil”. Lecture Notes in Civil Engineering, 112, 39-50.

Ali, N.A., Karkush, M.O. (2021). “Improvement of unconfined compressive strength of soft clay using microbial calcite precipitates”. Journal of Engineering, 27 (3), 67-75.

Almuaythir, S., Zaini, M.S., Hasan, M., and Hoque, M.I. (2024). "Sustainable soil stabilization using industrial waste ash: Enhancing expansive clay properties". Heliyon, 10 (20), e39124.

Aneke, I.F., Shamshad, A., Denis, K., and Siddiqua, S. (2024). "Enhancing dynamic shear resistance and efficient micro-void reduction of expansive soil using activated nano-desilicated fly ash". International Journal of Geo-synthetics and Ground Engineering, 10 (4), 72.

Attah, I.C., Okafor, F.O., and Ugwu, O.O. (2022). "Durability performance of expansive soil ameliorated with binary blend of additives for infrastructure delivery". Innovative Infrastructure Solutions, 7 (3).

Belihu, J., Teshome, G., Geremew, A., and Fayissa, B. (2025). "Experimental study on the stabilization of expansive soil with blended fine cinder gravel and waste marble dust: A case study of Jimma town". Jordan Journal of Civil Engineering, 19 (1), 128-144.

Chiu, A.C., Ibrahim, M.M., Ajamee, M.A., and Baguma, M.M. (2024) "Slope stability analysis of cement and silica fume stabilized expansive soil slope". IOP Conference Series: Earth and Environmental Science, 1336 (1).

Chu, C.F., Zhan, M.H., Feng, Q., Deng, Y.F., Li, D., Zha, F.S., and Hou, X.L. (2022). "Expansive soil modified by iron tailing sand and calcium carbide slag as sub-grade material". Environment, Development and Sustainability, 25, 10393-10410.

Dai, Z.J., Guo, J.H., Zhong, K., Tong, K.W., Li, S.C., Huang, K., and Chen, S.X. (2024). "Dynamic evolution of three-dimensional cracks in expansive soil under wet-dry cycles: Insights from resistivity monitoring". Bulletin of Engineering Geology and the Environment, 83, 305.

De, S.B., Bandeira, A.P., Santos, O.F., and Durante, I.M. (2024). "Using limestone mining waste to stabilize expansive soils in Ceará, Brazil". Geotechnical and Geological Engineering, 42, 2517-2528.

Dinan, A.A., Neebha, T.M., Umadevi, S., Anad, S., and Cashell, K.A. (2022). "Shrinkage crack detection in expansive soil using deep convolutional neural network and transfer learning". KSCE Journal of Civil Engineering, 26 (10), 4202-4213.

Duan, J.Y., Wu, J.J., Su, Y., Lin, Y.L., Li, Y.F., and Lu, L. (2024). "Shear behaviors of expansive soils over a wide confining pressure range and their impacts on strength parameters". Transportation Geotechnics, 48, 101328.

Elmashed, M.E., Sharaf, M., and Abdelaziz, T. (2022). "Improvement of swelling soil by using lime sludge and sodium chloride". Arabian Journal of Geosciences, 15, 1761.

Gunarti, A.S., Zaika, Y.L., Munawir, A., Surya, E.A., and Harimurti. (2023). "Identifying the micro-structure and mechanical properties of expansive soil stabilized using fly ash and waste foundry sand". Eastern-European Journal of Enterprise Technologies, 6 (6), 31-40.

Guo, J.H., Ding, G., and Wang, H.H. (2024). "Dynamic development law of expansive soil cracks under environmental influence". International Journal of Civil Engineering, 22, 787-800.

Guo, P.F., Wang, Y.Y., Zhang, X.Y., Ma, X.F., Deng, S.W., Zhu, X.Y., and Qiu, Y. (2024). "Investigation on elastic-plastic deformation and mechanical failure of varied-moisture expansive soil subjected to dry-wet cycles". Environmental Earth Sciences, 83, 433.

Habal, A.H., Medjnoun, A., Djerbal, L., and Bahar, R. (2024). "Mechanical and micro-structure behavior of expansive soil treated by lime-activated granulated blast furnace slag". Indian Geotech. J. (pre-publish), 1-17.

Han, L.W., Ji, W.H., Ma, L.Y., Guo, R.B., Zhang, Y.F., and Zhang, H.Y. (2024). "Microscopic mechanisms and evolution models of crack development in an expansive soil under conditions of rainfall evaporation cycles". Sustainability, 16 (17), 7617.

Huang, Z., Wei, B.X., Zhang, L.J., Chen, W., and Peng, Z.M. (2019). "Surface crack development rules and shear strength of compacted expansive soil due to dry-wet cycles". Geotech. Geol. Eng., 37, 2647-2657.

Janani, V., and Ravichandran, P.T. (2023). "Innovative natural admixture of calcined clay to improve strength and durability characteristics of expansive soil". Innovative Infrastructure Solutions, 8 (38).

Karkush, M.O., and Yassin, S. (2020). "Using sustainable material in the improvement of the geotechnical properties of soft clayey soil". Journal of Engineering Science and Technology, 15 (4), 2208-2222.

Liu, J.J., Yu, J.H., Hu, S.S., Hu, C.L., Wang, J.J., Yu, Z.W., and Huang, K. (2024). "Analysis of crack evolution of expansive soil embankment under extreme arid climate". Case Studies in Construction Materials, 20, e02902.

Luo, X.Q., Kong, L.W., Yan, J.B., Gao, Z., and Tian, S.K. (2024). "*In-situ* mechanical property and mechanism analysis of shallow expansive soil under the influence of water content and fissures". KSCE Journal of Civil Engineering, 28 (10), 4281-4292.

Melese, Damtew T. (2022). "Improvement of engineering properties of expansive soil modified with scoria". Jordan Journal of Civil Engineering, 16 (2), 211-218.

Ministry of Water Resources of China. (2019). "Geotechnical engineering test method and criterion: GB/T 50123-2019". Beijing: China Plan Publishing House (In Chinese).

Mobarezi, M., Nikooee, E., Owji, R., and Habibagahi, G. (2024). "Enzyme-induced carbonate precipitation as a novel remedy for expansive soils: Assessing microfabric and swelling characteristics". Geotechnical and Geological Engineering (pre-publish), 1-19.

Pachideh, G., Gholhaki, M., and Rezaifar, O. (2021). "Experimental study on engineering properties and micro-structure of expansive soils treated by lime containing silica nano-particles under various temperatures". Geotechnical and Geological Engineering, 39, 4157-4168.

Shivanshi, Jha, A.K., Singh, V.B., Jain, A.K., and Akhtar, M.P. (2022). "Effect of soluble gypsum on swell behaviour of lime-treated expansive soil: A micro-level investigation". Geomechanics and Geoengineering, 17 (6), 1786-1800.

Sun, D.X., Liu, X.F., Yuan, S.Y., Pan, G.F., Jiang, G.L., Wang, H.L., Hideo, K., and Buzzi, O. (2023). "Three-dimensional characterization of cracks in undisturbed mile expansive soil using X-ray computed tomography". Soils and Foundations, 63 (3), 101282.

Wang, J. (2024). "The impact of cement on the mechanical properties of expansive soil". Journal of Civil and Transportation Engineering, 1 (2).

Xu, J.J., Zhang, H., Tang, C.S., Yang, Y.W., Li, L., Wang, D.L., Liu, B., and Shi, B. (2024). "Soil desiccation crack recognition: New paradigm and field application". Journal of Geophysical Research: Machine Learning and Computation, 1 (3), e2024JH000347.

Zhang, Q., Xia, Y.J., Zhao, J.C., Tang, C.A., and Zhang, B. (2024). "Experimental investigation of crack evolution in expansive soil-rubber mixture (ESR) under freeze-thaw cycles". Cold Regions Science and Technology, 217, 104016.

Zhang, Y.G., Zhang, Z.B., Zhao, C.H., Zhang, Z.L., Kou, J.H., and Jing, Z. (2024). "Experimental study on engineering characteristics of cement-metakaolin composite-modified expansive soil". Academic Journal of Architecture and Geotechnical Engineering, 6 (4).

Zhao, N.F., Ye, W.M., Chen, Y.G., Chen, B., and Cui, Y.J. (2019). "Investigation on swelling-shrinkage behavior of unsaturated compacted GMZ bentonite on wetting-drying cycles". Bulletin of Engineering Geology and the Environment, 78, 617-627.

Zhao, Y., Zhang, H.R., Wang, G.Y., Yang, Y.Q., and Ouyang, M. (2024). "Development characteristics and mechanism of crack in expansive soil under wet-dry cycling". Applied Sciences, 14 (15), 6499.

Zhou, A.N., Du, J.P., Lin, X.S., Bu, Y.H., and Kodikara, J. (2023). "Nano-scale mechanism on lime stabilization of expansive soil". Acta Geotechnica, 18, 2681-2701.

Zhou, R., Wang, B.T., Han, S.Y., Wang, D.Y., and Zhang, F.H. (2024). "Mechanisms of crack development and strength deterioration in compacted expansive soils under controlled wetting-drying conditions". Engineering Failure Analysis, 159, 108133.

Zhu, H.X., Zhang, Y., Li, Z.H., and Xue, X.Y. (2021). "Study on crack development and micro-pore mechanism of expansive soil improved by coal gangue under drying-wetting cycles". Materials, 14, 6546.